Analysis and Design of Multiport Waveguide Junctions with Artificial Inclusions Made of Cylindrical Rods

Bogdanov, Faik
Communications Department, Georgian Technical University : Professor

Kevanishvili, Guram
Communications Department, Georgian Technical University : Professor

Kim, Dong Ill
Department of Radio Sciences and Engineering, Korea Maritime University : Professor

Jandieri, George
Communications Department, Georgian Technical University : Professor

他

https://doi.org/10.15017/1516216

出版情報：九州大学大学院システム情報科学紀要. 11 (1), pp.7-16, 2006-03-24. 九州大学大学院システム情報科学研究院
バージョン：
権利関係：

九州大学大学院
システム情報科学紀要
第11巻 第1号 平成18年3月

Research Reports on Information Science and
Electrical Engineering of Kyushu University
Vol.11, No.1, March 2006

Analysis and Design of Multiport Waveguide Junctions with Artificial Inclusions Made of Cylindrical Rods

Faik BOGDANOV*, Guram KEVANISHVILI*, Dong Ill KIM**,
George JANDIERI* and Kiyotoshi YASUMOTO***

(Received November 29, 2005)

Abstract: A rigorous electromagnetic theory is developed to analyze multiport waveguide junctions with artificial inclusions made of cylindrical rods and placed in the main arm. The scattering characteristics of a 3-port junction are discussed with the numerical examples for the SWR maps, the power reflection and transmission coefficients, and the 3D plots of near fields inside the junction area. A strategy to optimize matching properties of the 3-port waveguide junctions is also described.

Keywords: Waveguide junction, Artificial inclusions, Electrodynamic theory, Fourier transform, Optimization strategy

1. Introduction

Multiport waveguide junctions are widely used in microwave range to compose a number of microwave devices, such as directional couplers, power dividing circuits, multiplexers, filters, phase shifters and others[1)-2)]. The effectiveness of these devices is dependent on matching quality of waveguide arms, i. e. providing of high enough delivery of useful power to the desired arm and its suppression in remain arms. It is also important to provide the stable characteristics of these junctions in a wide frequency band.

Various techniques and methods have been developed during decades to investigate multifarious characteristics of multiport waveguide junctions[2)-25)]. Previous studies[2)-6)], carried out mainly for 3-port or T-junctions, were based on the coarse electrodynamics approaches and gave acceptable results only near a cut-off frequency. Many papers have then been published in last decades, which were devoted to the rigorous electrodynamic analysis of both simple, 3-port, T-junctions[7)-17)], and 4-port cruciform waveguide junctions as well[18)-22)]. More recently, multiport waveguide junctions in E- and H- planes simultaneously have been reported[23)-25)].

The previous investigations of waveguide junctions have revealed that the practically applicable matching of waveguide arms can be achieved only in a narrow frequency band and for fixed ratios of cross-sectional dimensions of waveguide arms. To improve matching properties of the junctions, it is necessary to properly modify the junction geometry by introducing artificial inclusions.

Various types of artificial inclusions, such as conducting strips, diaphragms, cylindrical rods, and dielectric layers, are used as adjusting elements for matching the waveguide sections with different properties[3)-4)]. Although the artificial inclusions in the conventional waveguide geometry are well studied[26)-33)], there arise several difficulties in the treatment when they are placed in the waveguide junctions. This is why the waveguide junctions with various artificial inclusions have not yet been analyzed enough[34)-36] and require the further efforts.

In this paper, a rigorous electromagnetic theory is developed to analyze multiport waveguide junctions with artificial inclusions made of cylindrical rods and placed in the main arm. The approach is based on the Fourier transform technique combined with the eigenmode expansion method and the image theory. The system of linear algebraic equations to calculate the scattering properties of the 3-port waveguide junction is obtained in closed form. Numerical examples for the power standing wave ratio maps, the power reflection and transmission coefficients, and the 3D-views of the near field structure are presented for the junction with a metallic or dielectric rod. A strategy to optimize the matching properties of the 3-port

* Communications Department, Georgian Technical University, Georgia, Professor
** Department of Radio Sciences and Engineering, Korea Maritime University, Korea, Professor
*** Department of Computer Science and Communication Engineering

waveguide junctions is also discussed.

2. Boundary Problem Formulation

The geometry of the problem to be considered is illustrated in **Fig. 1(a)**. It consists of 3-port H-plane waveguide junction with a circular rod placed in the main arm. Here a and b are widths of wider sides of the main and side waveguide arms, c is the radius of the rod, Δ is its separation from the left side wall of the main arm, ℓ is its distance from the juncture, and $L(=\ell+b)$ is its distance from the bottom of the side arms. The rod may be a perfect conductor or a dielectric. The origin of the Cartesian coordinate system is taken at the centre of cylinder. **Figure 1(b)** illustrates the 4-port H-plane waveguide junction as an extension of the 3-port junction.

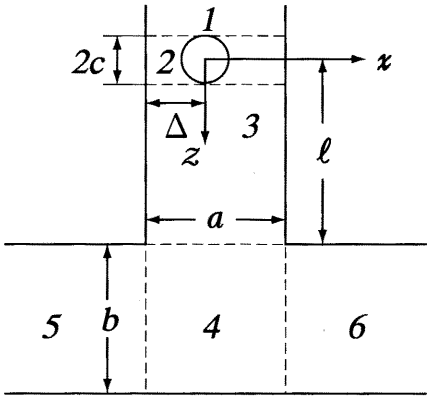

(a) 3-port junction

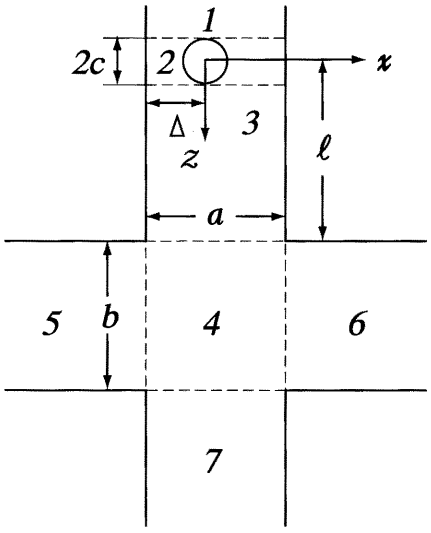

(b) 4-port junction

Fig. 1 Waveguide junctions with a cylindrical rod in the main arm: (a) 3-port junction and (b) 4-port junction.

We excite the inhomogeneous geometry of **Fig. 1** by the fundamental waveguide mode (TE_{10}) incident from the main arm *1* and seek for the electromagnetic field arisen in different areas of waveguide junction due to the diffraction on the rod and the juncture. For the sake of clarity and brevity, in this section, we consider in detail only geometry of **Fig. 1(a)**.

The incident wave in the main arm is fully defined by the y component of the electric field given by

$$E_y^{inc}=\sin\sigma_1(x+\Delta)\exp(-ih_1 z) \quad (-\Delta\le x\le a-\Delta,\ z\le 0) \tag{1}$$

where $h_1=(k^2-\sigma_1^2)^{1/2}$, $k=2\pi/\lambda$, $\sigma_1=\pi/a$, and $\mathrm{Im}\,h_1<0$. Hereinafter, time dependence is assumed to be $\exp(i\omega t)$. The total field in areas *1*, *2*, and *3* may be represented as Fourier series, whereas in areas *4*, *5*, and *6* as Fourier integrals in terms of modal spectra of reflected, transmitted, and interfering harmonics as follows:

$$E_{y1}=E_y^{inc}+\sum_{m=1}^{\infty}[A_m^-+B_m\exp(-ih_m\ell)]\sin\sigma_m(x+\Delta)\times\exp(ih_m z) \quad (z\le -c,\ -\Delta\le x\le a-\Delta) \tag{2a}$$

$$E_{y2}=E_y^{inc}+E_y^{sc}+\sum_{m=1}^{\infty}B_m\sin\sigma_m(x+\Delta)\times\exp[ih_m(z-\ell)] \quad (-c\le z\le c,\ -\Delta\le x\le a-\Delta) \tag{2b}$$

$$E_{y3}=E_y^{inc}+\sum_{m=1}^{\infty}\{A_m^+\exp(-ih_m z)+B_m\exp[ih_m(z-\ell)]\}\times\sin\sigma_m(x+\Delta) \quad (c\le z\le \ell,\ -\Delta\le x\le a-\Delta) \tag{2c}$$

$$E_{y4-6}=\int_{-\infty}^{\infty}dt\ F(t)\mathrm{sh}\left[\sqrt{t^2-k^2}(L-z)\right]\exp(itx) \quad (\ell\le z\le L,\ -\infty\le x\le\infty) \tag{2d}$$

where $h_m=\sqrt{k^2-\sigma_m^2}$, $\mathrm{Im}\,h_m<0$, $\sigma_m=m\pi/a$, and $L=\ell+b$. In (2a)-(2d), $\{A_m^-\}$ and $\{B_m\}$ are unknown Fourier amplitudes of modal spectra of waves reflected from the rod and the juncture, $\{A_m^+\}$ are those for the waves transmitted through the rod, and $F(t)$ are the amplitudes of continuous Fourier spectrum of waves transmitted to the resonance area *4* and two side arms *5* and *6*.

The field E_y^{sc} in (2b), scattered by the cylindrical rod, may be represented using the scattered field by the two-element periodic grating composed of mirror

images of the cylindrical rod in the left and right waveguide walls as follows:

$$E_y^{sc}=\sum_{\nu=-\infty}^{\infty}\sum_{m=-\infty}^{\infty}X_m[H_m^{(2)}(kr_\nu)\exp(im\varphi_\nu) -H_m^{(2)}(k\rho_\nu)\exp(-im\psi_\nu)] \quad (r_\nu\geq c,\ \rho_\nu\geq c) \tag{3}$$

where

$$r_\nu=\sqrt{z^2+(x-2a\nu)^2}$$
$$\varphi_\nu=\mathrm{arctg}\left(\frac{x-2a\nu}{z}\right) \tag{4a}$$
$$\rho_\nu=\sqrt{z^2+[x-2(a\nu+\Delta)]^2}$$
$$\psi_\nu=\mathrm{arctg}\left[\frac{x-2(a\nu+\Delta)}{z}\right] \tag{4b}$$

are local cylindrical coordinates of the real and image cylinders, $H_m^{(2)}$ is the m-th order Hankel function of the second kind and X_m are unknown amplitudes of multipole spectrum of scattered field.

The unknown coefficients A_m^-, A_m^+, B_m, $F(t)$, and X_m are determined from the boundary conditions which require that the E_y field should be zero on the surfaces of metallic rod ($r_0=d/2$, $0\leq\varphi_0\leq2\pi$) and two waveguide walls ($z\leq\ell$, $x=\pm a/2$), and the E_y and H_x fields should be continuous across the interfaces connecting the areas *1*, *2*, and *3* as follows:

$$E_{y1}=E_{y2} \quad (z=-c,\ -\Delta\leq x\leq a-\Delta) \tag{5a}$$
$$E_{y2}=E_{y3} \quad (z=c,\ -\Delta\leq x\leq a-\Delta) \tag{5b}$$
$$E_{y4}=\begin{cases}E_{y3}, & (-\Delta\leq x\leq a-\Delta,\ z=\ell)\\ 0, & (x\leq-\Delta,\ x\geq a-\Delta,\ z=\ell)\end{cases} \tag{5c}$$
$$\frac{\partial E_{y4}}{\partial z}=\frac{\partial E_{y3}}{\partial z}, \quad (-\Delta\leq x\leq a-\Delta,\ z=\ell). \tag{5d}$$

3. System of Functional Equations

To apply the boundary condition for E_y on the surface of cylindrical rod ($r_0=d/2$), E_y^{sc} given by (3) is transformed into the expression based on the coordinate (r_0, φ_0) by making use of the addition theorem for cylindrical functions. The result is substituted into (2b) to obtain the following equation for the coefficients X_m and B_m:

$$\sin\left[\frac{\pi}{a}\left(\frac{d}{2}\sin\varphi_0+\Delta\right)\right]\exp(-ih_1\cos\varphi_0) +\sum_{m=-\infty}^{\infty}X_m\left\{H_m^{(2)}\left(\frac{kd}{2}\right)\exp(im\varphi_0) +\sum_{s=-\infty}^{\infty}J_s\left(\frac{kd}{2}\right)[-i^{s-m}H_{s+m}^{(2)}(2k\Delta)+Z_{s-m}(2ka,0) -(-1)^mZ_{s+m}(2ka,2k\Delta)]\exp(is\varphi_0)\right\}$$
$$+\sum_{m=1}^{\infty}B_m\exp(-ih_m\ell)\sin\left[\sigma_m\left(\frac{d}{2}\sin\varphi_0+\Delta\right)\right] \times\exp(ih_m\cos\varphi_0) \quad (0\leq\varphi_0\leq2\pi) \tag{6}$$

with

$$Z_m(u,w)=i^m\sum_{\nu=1}^{\infty}H_m^{(2)}(\nu u+w) +i^{-m}\sum_{\nu=1}^{\infty}H_m^{(2)}(\nu u-w) \tag{7}$$

where $J_s(x)$ is the s-th order Bessel function. Note that E_y fields defined by (2a)-(2c) together with (3) automatically satisfy the boundary conditions on the waveguide walls at $x=-\Delta$ and $x=a-\Delta$.

Next, applying the boundary conditions (5a) and (5b), the following relations between the modal coefficients $A_p^\pm$ and multipole coefficients X_m are derived:

$$A_p^\pm=\frac{4}{h_pa}\sum_{m=-\infty}^{\infty}\begin{cases}i^{\pm m}\sin(\sigma_p\Delta\pm m\,\mathrm{arctg}\,\xi_p)X_m, & (p<[D])\\ \frac{1}{2i}\{(-1)^m\exp(i\sigma_p\Delta\mp m\xi'_p) -\exp[-(i\sigma_p\Delta\mp m\xi'_p)]X_m\} & (p>[D])\end{cases} \tag{8}$$

with

$$\xi_p=\mathrm{Atan}\left(\frac{p}{\sqrt{D^2-p^2}}\right),\quad \xi'_p=\mathrm{Arth}\left(\frac{\sqrt{D^2-p^2}}{p}\right) \tag{9}$$

where $D=2a/\lambda$.

Finally, we apply the boundary conditions (5c) and (5d) to obtain the following functional equations for the coefficients A_m^+, B_m, and $F(t)$:

$$\int_{-\infty}^{\infty}dt\,F(t)\mathrm{sh}[\alpha(t)b]\exp(itx) =\begin{cases}\sum_{m=1}^{\infty}[B_m+(\delta_{m1}+A_m^+)\exp(-ih_m\ell)]\sin\sigma_m(x+\Delta) & (-\Delta\leq x\leq a-\Delta)\\ 0 & (x\leq-\Delta \text{ and } x\geq a-\Delta)\end{cases} \tag{10}$$

$$\int_{-\infty}^{\infty}dt\,\alpha(t)F(t)\mathrm{ch}[\alpha(t)b]\exp(itx) =-\sum_{m=1}^{\infty}ih_m[B_m-(\delta_{m1}+A_m^+)\exp(-ih_m\ell)] \times\sin\delta_m(x+\Delta) \quad (-\Delta\leq x\leq a-\Delta) \tag{11}$$

where $\alpha(t)=\sqrt{t^2-k^2}$. Equations (6), (10), and (11) together with (8) yield a set of functional equations to determine the unknowns X_m, $A_m^\pm$, B_m, and $F(t)$ under the excitation by the TE_{10} mode field (1).

4. Reduced System of Functional Equations

Let now transform the system of functional equations (6), (10), and (11) to the reduced one which is more convenient for the numerical analysis. First, using the orthogonality of transverse eigen-functions $\{\sin\sigma_n(x+\Delta)\}_{n=1}^{\infty}$ on the segment $-\Delta\leq x\leq a-\Delta$ and the filtration properties of Dirac δ -function on interval $-\infty<x<\infty$, (10) can be rearranged to obtain the relation between the coefficients $F(t)$ and (A_m^+, B_m) as follows:

$$F(t)=\frac{1}{2\pi\mathrm{sh}[a(t)b]}\times\sum_{m=1}^{\infty}[B_m+(\delta_{m1}+A_m^+)\exp(-ih_m\ell)]\Phi_m(t) \quad (12)$$

where

$$\Phi_m(t)=\frac{\sigma_m}{\sigma_m^2-t^2}\exp(it\Delta)[1-(-1)^m\exp(-ita)]. \quad (13)$$

Substituting (12) into (11), we have the following functional equation which relates the unknowns B_m and A_m^+:

$$\sum_{m=1}^{\infty}[B_m+(\delta_{m1}+A_m^+)\exp(-ih_m\ell)]G_m(x)=\sum_{m=1}^{\infty}ih_m[B_m-(\delta_{m1}+A_m^+)\exp(-ih_m\ell)]\times\sin\delta_m(x+\Delta) \quad (-\Delta\leq x\leq a-\Delta) \quad (14)$$

where

$$G_m(x)=\frac{1}{2\pi}\int_{-\infty}^{\infty}dt\frac{a(t)\Phi_m(t)\mathrm{ch}[a(t)b]}{\mathrm{sh}[a(t)b]}\exp(itx). \quad (15)$$

The integration in (15) can be easily performed using the residual calculus and leads to

$$G_m(x)=\sigma_m\left\{\frac{\sqrt{\sigma_m^2-k^2}}{\sigma_m}\mathrm{cth}(\sqrt{\sigma_m^2-k^2}\,b)\sin\sigma_m(x+\Delta)+i\sum_{n=1}^{\infty}\frac{t_n^2-k^2}{bt_n(\sigma_m^2-t_n^2)}\times[\exp(it_n(x+\Delta))-(-1)^m\exp(it_n[a-(x+\Delta)])]\right\} \quad (16)$$

where $t_n=-\sqrt{k^2-q_n^2}$ and $q_n=\pi n/b$.

5. System of Algebraic Equations

Our aim is now to solve the key system of functional equations (6) and (14) with the substitution of (8). For this purpose, (6) is multiplied by the complete system of azimuthal functions $\{\exp(-in\varphi_0)\}_{n=0,\pm1,\pm2,\cdots}$ and integrated over $0\leq\varphi_0\leq2\pi$, whereas (14) is multiplied by the transverse eigen-functions of the main waveguide arm $\{\sin\sigma_n(x+\Delta)\}_{n=1}^{\infty}$ and integrated over $-\Delta\leq x\leq a-\Delta$. As a result, we arrive at the key dual system of algebraic equations for the unknown coefficients B_p and X_m as follows:

$$X_n+\sum_{m=-\infty}^{\infty}P_{nm}X_m+\sum_{p=1}^{\infty}r_{np}B_p=a_n \quad (17a)$$

$$-B_\mu+\sum_{m=-\infty}^{\infty}\tilde{g}_{\mu m}X_m+\sum_{p=1}^{\infty}\tilde{Q}_{\mu p}B_p=b_\mu \quad (17b)$$

$$(n=0, \pm1, \pm2, \ldots; \quad \mu=1, 2, 3, \ldots)$$

with

$$a_n=-i^{-n}\sin(\sigma_1\Delta+n\xi_1)\frac{J_n(kc)}{H_n^{(2)}(kc)} \quad (18)$$

$$b_\mu=-(\tilde{Q}_{\mu1}+\delta_{\mu1})\exp(-ih_1\ell) \quad (19)$$

$$\tilde{Q}_{\mu p}=i2\frac{Q_{\mu p}}{h'_\mu a} \quad (20)$$

$$Q_{\mu p}=\sigma_p\left\{\frac{\zeta_p}{\sigma_p\mathrm{th}(\zeta_p b)}\frac{a}{2}\delta_{\mu p}-i\frac{\sigma_n}{b}\sum_{s=1}^{\infty}\frac{(h'^2_s-k^2)[(-1)^\mu-\exp(-ih'_s a)]}{h'_s(h'^2_s-\sigma_\mu^2)(h'^2_s-\sigma_p^2)}\times[(-1)^\mu+(-1)^p]\right\} \quad (21)$$

$$r_{np}=\frac{J_n(kc)}{H_n^{(2)}(kc)}\exp(-ih_p\ell)\times\begin{cases}i^n\sin(\sigma_p\Delta-n\xi_p) & (p<[D])\\ \frac{1}{2i}[\exp(i\sigma_p\Delta+n\xi'_p) & \\ -(-1)^n\exp(-(i\sigma_p\Delta+n\xi'_p))] & (p>[D])\end{cases} \quad (22)$$

$$P_{nm}=\frac{J_n(kc)}{H_n^{(2)}(kc)}[-i^{n-m}H_{n+m}^{(2)}(2k\Delta)+Z_{n-m}(2ka, 0)-(-1)^mZ_{n+m}(2ka, 2k\Delta)] \quad (23)$$

$$\tilde{g}_{\mu m}=\frac{4e^{-ih_\mu\ell}}{h_\mu a}\left[g_{\mu m}+\sum_{p=1}^{\infty}g_{pm}\tilde{Q}_{\mu p}\right] \quad (24)$$

$$g_{\mu m}=\begin{cases}i^m\sin(\sigma_\mu\Delta+m\xi_\mu) & (p<[D])\\ \frac{1}{2i}[(-1)^m\exp(i\sigma_\mu\Delta-m\xi'_\mu) & \\ -\exp(-(i\sigma_\mu\Delta-m\xi'_\mu))] & (p>[D])\end{cases} \quad (25)$$

where $\zeta_p=\sqrt{\sigma_p^2-k^2}$, $h_\mu=\sqrt{k^2-\sigma_\mu^2}$, and $h'_\mu=\sqrt{k^2-q_\mu^2}$. The extension of the present analysis to the 4-port junction as shown in **Fig. 1 (b)** is straightforward. We may introduce another unknown Fourier spectrum function into (2d) and another set of unknown modal amplitudes describing the transmitted field in the arm guide 7. The boundary-value matching procedure similar to that used for (2c) and (2d) is applied to the E_y field on $z=L$.

6. Extension of Solutions to Dielectric Rod Inclusion

If the circular rod consists of a dielectric with permittivity ε, we describe the E_y field inside the rod as

$$E_y^{inside}=\sum_{m=-\infty}^{\infty} Y_m J_m(k'r)\exp(im\varphi_0) \quad \left(r\le\frac{d}{2}\right) \tag{26}$$

where $k'=k\sqrt{\varepsilon/\varepsilon_0}$ and $\{Y_m\}$ are new unknowns to be found. The boundary conditions on the surface of the dielectric rod are given by

$$\begin{cases} E_{y2}=E_y^{inside} \\ \dfrac{\partial E_{y2}}{\partial z}=\dfrac{\partial E_y^{inside}}{\partial z} \end{cases} \quad \left(r=\frac{d}{2},\ 0\le\varphi\le 2\pi\right). \tag{27}$$

Applying the boundary conditions (5a)-(5d) together with (27), the solution again leads to the algebraic system (17) with the following replacement in (18), (22), and (23):

$$\frac{J_n(kc)}{H_n^{(2)}(kc)} \Rightarrow \frac{J_n(kc)J_n'(k'c)-W_rJ_n'(kc)J_n(k'c)}{H_n^{(2)}(kc)J_n'(k'c)-W_rH_n'^{(2)}(kc)J_n(k'c)} \tag{28}$$

where $W_r=\sqrt{\varepsilon_0/\varepsilon}$. The unknowns Y_m are related to the multipole coefficients X_m as follows:

$$Y_m=\frac{2i}{\pi kc[J_n'(kc)J_n(k'c)-J_n(kc)J_n'(k'c)/W_r]}X_m \tag{29}$$

The replacement of (28) and the relation (29) are enough to account dielectric properties of the rod inclusion.

7. Field in the Side Branches and Power Balance Equation in Waveguide Tee

The fields in the areas *1*, *2*, and *3* of the main arm of the junction may be calculated by substituting the solutions to the algebraic system (8) and (17) into (2a)-(2c). The calculation of the fields in the side branches requires additional analytical treatment. Substituting (12) into (2d), we have

$$E_{y4-6}=\sum_{m=1}^{\infty}[B_m+(\delta_{m1}+A_m^+)\exp(-ih_m\ell)]\Psi_m(x,z) \quad (\ell\le z\le L,\ -\infty<x<\infty) \tag{30}$$

with

$$\Psi_m(x,z)=\frac{\sigma_m}{2\pi}\int_{-\infty}^{\infty}dt\frac{\mathrm{sh}[a(t)(L-z)]}{\mathrm{sh}[a(t)b]}\times\frac{\exp(it(x+\Delta))-(-1)^m\exp(it[x-(a-\Delta)])}{\sigma_m^2-t^2} \tag{31}$$

where (8) has been used. The expression (31) is applied for all areas *4*, *5*, and *6* in side waveguide, but the result of integration is dependent on the area concerned. The integration of (31) in the resonance area *4* yields

$$\Psi_m(x,z)=\sin\sigma_m(x+\Delta)\frac{\mathrm{sh}[\zeta_m(L-z)]}{\mathrm{sh}(\zeta_m b)}-\frac{i\sigma_m}{b}\sum_{n=1}^{\infty}\frac{q_n\sin[q_n(L-z)]}{(-1)^n h_n' b(h_n'^2-\sigma_m^2)}\times\{\exp[-ih'(x+\Delta)]-(-1)^m\exp[-ih'(a-(x+\Delta)]\} \quad (-\Delta\le x\le a-\Delta). \tag{32}$$

In areas *5* and *6*, (31) is integrated to obtain

$$\Psi_m(x,z)=-i\sigma_m\sum_{n=1}^{\infty}\frac{q_n(-1)^n}{bh_n'(h_n'^2-\sigma_m^2)}\times\{\exp(\mp ih_n'\Delta)-(-1)^m\exp[\pm ih_n'(a-\Delta)]\}\times\sin[q_n(L-z)]\exp(\pm ih_n'x) \tag{33}$$

where "+" and "−" signs in the exponent stand for areas *5* ($x<-a/2$) and *6* ($x>a/2$), respectively.

The formula (32) represents the standing waves in resonance area *4*, while the formulas (33) represents the outgoing waves in side waveguide arms *5* and *6*. Substituting (33) into (30) and changing the order of the summations, the transmitted fields in the side arms are derived as follows:

$$E_{y5,6}=\sum_{n=1}^{\infty}T_n^{\mp}\sin[q_n(L-z)]\exp(\pm ih_n'x) \quad (\ell\le z\le L,\ |x|\ge a/2) \tag{34}$$

with

$$T_n^{\mp}=(-1)^n i\frac{q_n}{bh_n'}\sum_{m=1}^{\infty}[B_m+(\delta_{m1}+A_m^+)\exp(-ih_m\ell)]\times\{\exp(\mp ih_n'\Delta)-(-1)^m\exp[\pm ih_n'(a-\Delta)]\}\times\frac{\sigma_m}{h_n'^2-\sigma_m^2} \tag{35}$$

where T_n^- and T_n^+ indicate the amplitudes of the modal fields transmitted into the side waveguide arms *5* and *6*, respectively.

The field representations (1), (2a), and (30) allows the derivation of power balance equation in waveguide tee as follows:

$$P_{refl}+P_{left}+P_{right}=1 \tag{36}$$

with

$$P_{refl}=\sum_{m=1}^{M} P_{1m} \tag{37a}$$

$$P_{left}=\sum_{n=1}^{N} P_{5n} \tag{37b}$$

$$P_{right}=\sum_{n=1}^{N} P_{6n} \tag{37c}$$

$$P_{1m}=\frac{h_m}{h_1}|A_m|^2 \tag{38a}$$

$$P_{5,6n}=\frac{h'_n b}{h_1 a}|T_n^{\mp}|^2 \tag{38b}$$

where P_{refl}, P_{left}, and P_{right} represent the power reflection and transmission coefficients in the main and side waveguide arms, respectively, while M and N denote the number of propagating modes in these arms. The equation (36) may be used to estimate fidelity of the obtained solution from the energy conservation point of view.

8. Numerical Results

The developed theory has been used to create a user-friendly program package which can calculate various electrodynamic characteristics of the waveguide junctions such as the reflection coefficient, the reflected and transmitted powers, the 3D plots of near fields isolines inside the junction area, the animation of the near field, and the power standing wave ratio (SWR) maps. Using the created program tools, an optimization strategy has been developed to find the geometrical parameters of the junction ensuring a minimum reflection in the desired frequency band.

In what follows we shall demonstrate several simulation results for the case of metallic and dielectric rods symmetrically placed ($\Delta=a/2$) in the main arm of the 3-port waveguide junction with $b/a=1$. These results have been obtained by truncating the dual system of algebraic equations (17a) and (17b) up to $N_{tr}=5$ for both eigenmode (2) and multipole (3) expansions of the waveguide fields. In calculation of slowly convergent series (7), we left $N_s=100$ terms in the series and used for the rest the original procedure developed in 38).

First, we shall demonstrate the results for the case of metallic rod symmetrically placed in the main arm of the 3-port waveguide junction. The SWR maps in the main arm versus the rod parameters ℓ/a and d/a are plotted in **Figs. 2(a)** and **2(b)** for $2a/\lambda=1.74$ and $2a/\lambda=2.5$ where $d(=2c)$ denotes the diameter of the rod. The indicated frequency parameters $2a/\lambda=1.74$ and $2a/\lambda=2.5$ correspond the central frequencies of the bandwidths providing the one-mode regime and two-modes regime of wave propagation, respectively. The shadow in palette maps indicates the definite levels of standing wave ratio which are shown on the scroll bars on the right. Therefore the minimum SWR (minimum reflection) in the main arm is realized in the central black area of the maps. For instance, **Fig. 2(a)** shows that the minimum reflection in the one-mode regime is obtained for the rod param-

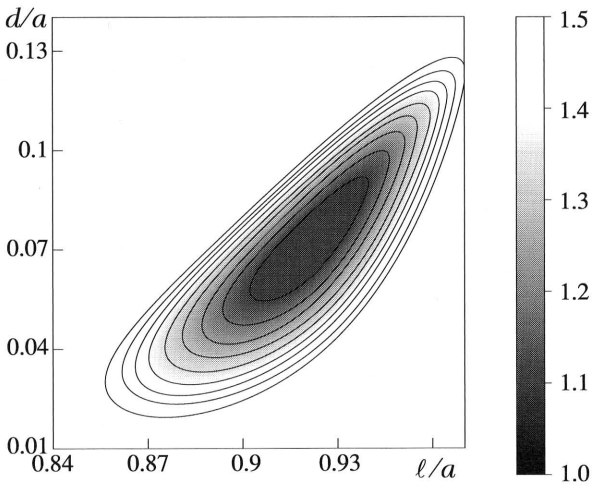

(a) $2a/\lambda=1.74$

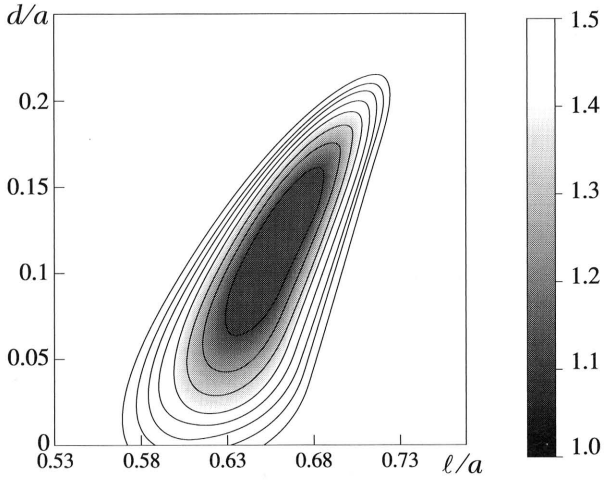

(b) $2a/\lambda=2.5$

Fig. 2 SWR maps of the 3-port waveguide junction with a symmetric metallic rod for two different frequency parameters: (a) $2a/\lambda=1.74$ for one-mode regime and (b) $2a/\lambda=2.5$ for two-modes regime.

eters $\ell/a=0.92$ and $d/a=0.07$.

The SWR maps versus frequency parameter $2a/\lambda$ and one of two rod parameters, being fixed the other to the optimized values $\ell/a=0.92$ or $d/a=0.07$, are plotted in **Figs. 3(a)** and **3(b)**. These maps are useful to correct the optimal values of the rod parameters and to determine the frequency bandwidth providing the admissible maximum level of SWR. The larger this admission, the larger frequency bandwidth is available.

Figure 4 shows the power reflection coefficient P_{refl} in the main arm *1* and the power transmission coefficients P_{left} and P_{right} in the side waveguides *5* and *6* as functions of the frequency parameters $2a/\lambda$, where the rod parameters are assumed to be the optimal values $\ell/a=0.92$ and $d/a=0.07$. In the present case with $\Delta=a/2$, we have $P_{left}=P_{right}$ because the geometry of the junction is symmetric with respect to $x=0$. We can see that the numeral data of P_{refl}, P_{left}, and P_{right} well satisfy the power conservation relation (36). **Figure 4** is useful to design the available frequency bandwidth with admissible reflection.

The near field structure is instructive to understand the reasonable peak values of electric field near the resonance region and the formation process of the regular field distribution nearby the juncture. **Figure 5** shows the 3D-view of the E_y field structure around the junction area where $\ell/a=0.92$, $d/a=0.07$, and $2a/$

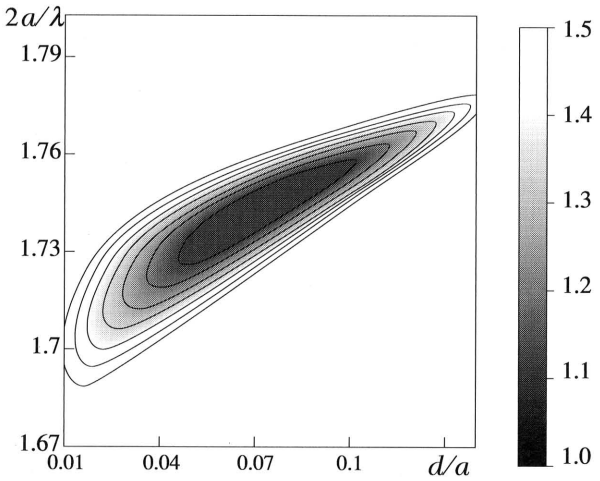

(a) $\ell/a=0.92$

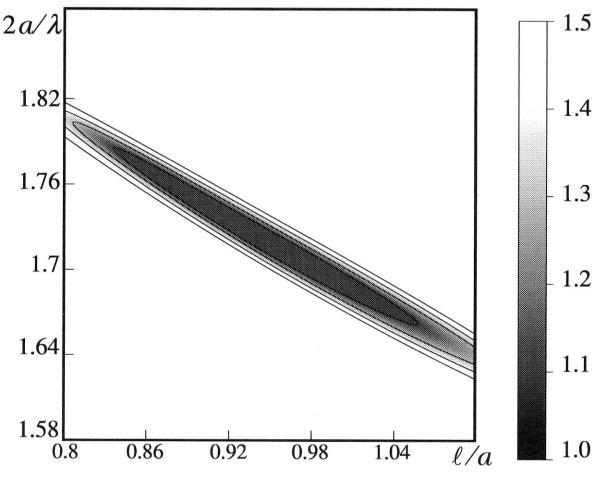

(b) $d/a=0.07$

Fig. 3 SWR maps of the 3-port waveguide junction with a symmetric metallic rod for different rod parameters: (a) $\ell/a=0.92$ and (b) $d/a=0.07$.

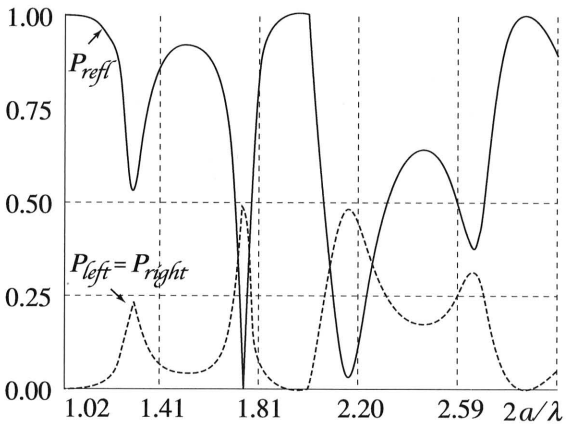

Fig. 4 Power reflection and transmission coefficients as functions of frequency parameters $2a/\lambda$ for the 3-port waveguide junction with a symmetric metallic rod where $\ell/a=0.92$ and $d/a=0.07$.

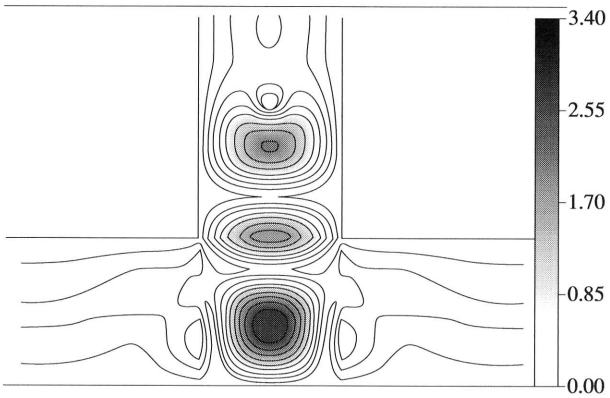

Fig. 5 3D-view of the electric field structure in the 3-port waveguide junction with a symmetric metallic rod at optimal rod parameters: $\ell/a=0.92$, $d/a=0.07$, and $2a/\lambda=1.74$.

λ=1.74. We can visually understand how the incident field is transmitted through the circular rod, resonate in the resonance area *4*, and is transmitted into the arm waveguides *5* and *6* to form the regular waveguide modes.

Next, we consider the case of the 3-port waveguide junction with a circular dielectric rod placed in the main arm. The numerical results of the SWR maps, the power reflection and transmission coefficients, and a 3D-view of the near field structure are plotted in **Fig. 6** to **Fig. 8**, respectively, for $\varepsilon/\varepsilon_0$= 3.8 and other indicated parameters. Comparing the results with those of **Fig. 3** to **Fig. 4**, we note that in the case of the dielectric rod, there exist a variety of optimal parameter sets providing the minimum SWR, while the frequency bandwidth becomes narrower than the case of metallic rod. **Figure 8** shows that the minimum reflection is associated with the larger peak values of electric field in resonance region. The use of the dielectric rod as a matching element is useful for flexibly designing the 3-port waveguide junction.

Before concluding, it is worth mentioning that the present theory and optimization strategy can be easily extended on a 3-port or 4-port waveguide junction with multiple rods. The integration of metallic and dielectric properties in the matching elements will allow one designing various microwave devices with

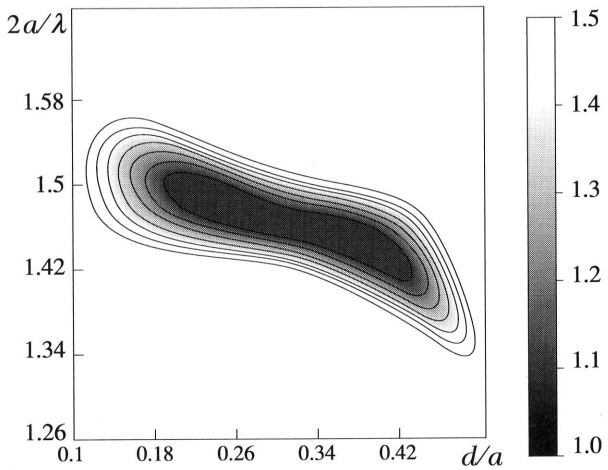

(a) ℓ/a=0.7

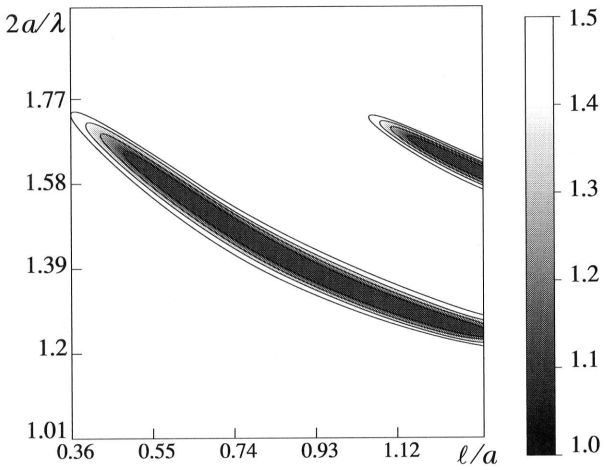

(b) d/a=0.24

Fig. 6 SWR maps in the 3-port waveguide junction with a symmetric dielectric rod of $\varepsilon/\varepsilon_0$=3.8 for different rod parameters: (a) ℓ/a=0.7 and (b) d/a=0.24.

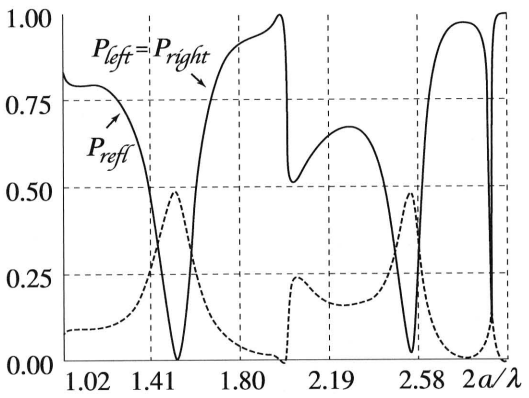

Fig. 7 Power reflection and transmission coefficients as functions of frequency parameters $2a/\lambda$ for the 3-port waveguide junction with a symmetric dielectric rod at optimal rod parameters metallic rod where $\varepsilon/\varepsilon_0$=3.8, ℓ/a=0.7, and d/a=0.24.

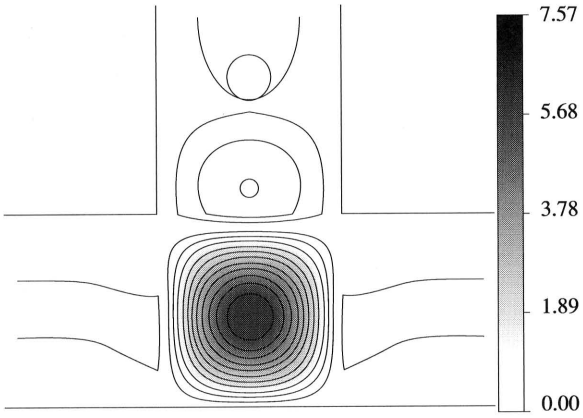

Fig. 8 3D-view of the electric field structure in the 3-port waveguide junction with a symmetric dielectric rod at optimal rod parameters: ℓ/a =0.7, d/a=0.24, and $2a/\lambda$=1.511.

desired properties.

9. Conclusion

A rigorous electromagnetic theory has been developed to analyze multiport waveguide junctions with artificial discontinuities made of cylindrical rods. The scattering characteristics of a 3-port junction were discussed in detail with the numerical examples for the SWR maps, the power reflection and transmission coefficients, and the 3D-plots of near fields inside the junction area. A strategy to optimize matching properties of the 3-port waveguide junctions was also described.

The developed theory and optimization strategy may be easily extended to more complicated geometries of waveguide junctions including multiple cylindrical rods and implemented to design various microwave devices.

Acknowledgment

This research was performed in part under supporting of International Science and Technology Center (ISTC) research team "Analysis and Design of Multiport Waveguide Junctions and Branchings with Improved Matching Characteristics" (grant G-871-2003). The authors would like to thank the ISTC for financially supporting this work.

References

1) F. Arndt, I. Ahrens, U. Papziner, U. Wiechmann and R. Willkeit: "Optimized E-plane T-junction Series Power Deviders," IEEE Trans. Microwave Theory Technol., Vol. MTT-35, pp.1052-1059 (1987).
2) F. Alessandri, M. Mongiardo and R. Sorrentino: "Computer-aided Design of Beam Forming Networks for Modern Satellite Antennas," IEEE Trans. Microwave Theory Technol., Vol.40, pp.1117-1127 (1992).
3) L. Lewin: Advanced Theory of Waveguides, Iliffe, London (1951).
4) A.F. Harvey: Microwave Engineering, Academic Press, London and New York (1963).
5) J.T. Allanson, R. Cooper and T.G. Cowling: "The Theory and Experimental Behaviour of Right-Angled Junctions of Rectangular Section Waveguide," J. IEE., Vol. 93, no 23, pp.177-187 (1946).
6) L. Lewin: Theory of Waveguides: Techniques for the Solution of Waveguide Problems, London, UK (1975).
7) E.A. Kuhn: "Mode-matching Method for Solving Field Problems in Waveguide and Resonator Circuits," AEU, Arch. Elek. Ubertragung., Vol.27, H-12, pp.511-518 (1973).
8) B.M. Mashkovtsev, K.N. Tsibizov and B.F. Emelin: Waveguide theory. Moscow, Nauka (1966) (in Russian).
9) G.Sh. Kevanishvili: "To the Theory of Waveguide Tee," Izvestia vuzov. Radiophysics, Vol.21, no.11, pp.1669-1674 (1978) (in Russian).
10) V.V. Nikolski and O.A. Golovanov: "Application of AMB Method for Modelling Waveguide Elements," In the book: Computer Design of Microwave Systems and Structure, Moscow: MIREA, pp.147-164 (1979) (in Russian).
11) L.A. Rud: "Wave Diffraction on T-junction of Rectangular Waveguides in H Plane," Radiotekhnika i Electronika, Vol.29, no.9, pp.1711-1719 (1984) (in Russian).
12) V.S. Mikhalevski, M.L. Pereiaslavets, Yu.M. Sinel'nilov and G.P. Siniavskii: "T-junction of Rectangular Waveguides," Radiotekhnika i Electronika, Vol.27, no. 8, pp.1478-1485 (1982) (in Russian).
13) S.V. Baraev and O.P. Korovin: "Calculation of Scattering Matrices of Waveguide Tee in E-plane," Radiotekhnika i Electronika, Vol.30, no.9, pp.1840-1842 (1985) (in Russian).
14) F.G. Bogdanov, G.Sh. Kevanishvili and G.G. Chikhladze: "Investigation of Electrodynamic Properties of Waveguide Tees," In the book: Waves and diffraction-90. Proceedings of X All-Union Symposium. (Vinnitsa, 1990). Moscow, Vol.3, pp.234-237 (1990) (in Russian).
15) F.G. Bogdanov, G.Sh. Kevanishvili and G.G. Chikhladze: "Electrodynamic Theory of Waveguide Tee in E-plane," Gorkii, 13 p. (Preprint /Edit. by Journal Izvestia vuzov. Radiophysics, deposition in VINITI, 21.02.1991; no.858-V91) (1991) (in Russian).
16) F.G. Bogdanov, G.Sh. Kevanishvili and G.G. Chikhladze: "To the Theory of Waveguide T-Junction in E-plane," Bulletin of the Academy of Sciences of Georgia, Vol. 141, no.1, pp.93-96 (1991) (in Russian).
17) F. Alessandri, M. Mongiardo and R. Sorrentino: "Rigorous Mode Matching Analysis of Mitered E-plane Bends in Rectangular Waveguide," IEEE Microwave and Guide Wave Letters, Vol.4, pp.408-410 (1994).
18) I.G. Prokhoda and V.P. Chumachenko: "Method of Partial Crossing Areas for Investigation of Waveguide-resonator Systems of Complicated Shape," Izvestia vuzov. Radiophysics, Vol.16, no.10, pp.1578-1582 (1973) (in Russian).
19) I.G. Prokhoda and V.P. Chumachenko: "Calculation of Four-arm Junction of Rectangular Waveguides in H-plane," Izvestia vuzov. Radioelectronics, Vol.16, no.10, pp.143-144 (1973) (in Russian).
20) I.G. Prokhoda, V.P. Lozianoi and V.M. Onufrienko at all.: Propagation of Electromagnetic Waves in Inhomogeneous Waveguide Systems. Dnepropetrovsk: Edit by DSU (1977) (in Russian).
21) I.G. Prokhoda and V.A. Karlov: "Matching of Cruciform Junction of Rectangular Waveguides in E-plane,"

Izvestia vuzov. Radioelectronics, Vol.29, no.2, pp.90-92 (1986) (in Russian).

22) F.G. Bogdanov, G.Sh. Kevanishvili and G.G. Chikhladze: "Diffraction Properties of Cruciform Junction of Rectangular Waveguides in E-plane," Radiotekhnika i Electronika. Vol.37, no.4, pp.659-667 (1991) (in Russian).
23) T. Sieverding and F. Arndt: "Modal Analysis of the Magic Tee," IEEE Microwave and Guide Wave Letters, Vol.3, pp.150-152 (1993).
24) H. Jia, K. Yoshitomi and K. Yasumoto: "Rigorous Analysis of Rectangular Waveguide Junctions by Fourier Transform Technique," Progress in Electromagnetic Research, PIER, Vol.20, pp.261-280 (1998).
25) H. Jia, K. Yoshitomi and K. Yasumoto: "Rigorous Analysis of E-/H- Plane Junctions in Rectangular Waveguides Using Fourier Transform Technique," J. Electromagnetic Waves and Applications, Vol.13, pp. 809-810 (1999), Progress in Electromagnetic Research, PIER Vol.21, pp.273-292 (1999).
26) A.L. Fel'dshtein, L.K. Iavich and V.P. Smirnov: Handbook on waveguide technology elements, Moscow, Gosenergoizdat (1967) (in Russian).
27) Yu. Shvinger: "Inhomogeneities in Waveguides," Foreign Radioelectronics, no.3, pp.3-106 (1970). Microwaves, Moscow, Nauka, 1985 (in Russian).
28) B.Yu. Kapilevich: "Dielectric Cylinder in a Rectangular Waveguide," Radiotekhnika i Electronika, Vol.33, no.4, pp.98-100 (1978) (in Russian).
29) G.Sh. Kevanishvili: "Diffraction of H_{10} Wave on Inductive Rod," Radiotekhnika i Electronika, Vol.20, no.9, pp. 1810-1817 (1975) (in Russian).
30) F.G. Bogdanov, G.Sh. Kevanishvili, G.V. Kekelia and N. M. Kurdiani: "Scattering of H_{10} Wave on Coaxial Metal-dielectric Rod," Diffraction of Electromagnetic Waves /Edit by Georgian Technical University, no.6 (335), pp.5-8 (1988) (in Russian).
31) F.G. Bogdanov, G.Sh. Kevanishvili and G.V. Kekelia: "Scattering of H_{10} Wave by the Set of Dielectric Cylinders in Rectangular Waveguide," Bulletin of the Academy of Sciences of Georgian SSR, Vol.130, no.3, pp.537 -540 (1988) (in Russian).
32) F.G. Bogdanov, G.Sh. Kevanishvili and G.V. Kekelia: "Analysis of Near Field of H_{10} Wave Diffraction by a Dielectric Cylinder in Rectangular Waveguide," Bulletin of the Academy of Sciences of Georgian SSR, Vol. 131, no.1, pp.61-63 (1988) (in Russian).
33) F.G. Bogdanov, G.Sh. Kevanishvili and G.G. Chikhladze: "Transmission of H_{10} Wave Through the Dielectric Layer With Inductive Bar," Bulletin of the Academy of Sciences of Georgia, Vol.141, no.2, pp.317-320 (1991) (in Russian).
34) F.G. Bogdanov, G.Sh. Kevanishvili, G.V. Jandieri, G.V. Kekelia and K. Yasumoto: "Simulation and Analysis of Multiport Waveguide Junctions with Artificial Discontinuities Formed of the Inductive Strips and Diaphragms," in Progress in Electromagnetic Research Symposium (PIERS-2004), Pisa, Italy, March, pp.125 -128 (2004).
35) F.G. Bogdanov, G.Sh. Kevanishvili, G.V. Jandieri and Dong Il Kim: "Simulation and Optimization of Waveguide Junctions with Artificial Discontinuities Including Strips and Dielectric Layer," Proc. IX International Seminar/Workshop on Direct and Inverse Problems of Electromagnetic and Acoustic Wave Theory (DIPED-2004, IEEE Catalog Number: 04TH8747), Lviv-Tbilisi, pp.47-50 (2004).
36) F.G. Bogdanov, G.Sh. Kevanishvili, G.V. Jandieri and K. Yasumoto: "Optimization Strategy for Multiport Waveguide Junctions with Canonical Types of Artificial Discontinuities," Proc. X International Symposium on Microwave and Optical Technology (ISMOT-2005), Fukuoka, Japan, pp.625-627 (2005).
37) R.F. Harrington: Field Computation by Moment Methods, IEEE Press, New York (1993).
38) G.Sh. Kevanishvili, O.P.Tsagareishvili: "The Method of Orthogolalization in The Diffraction Theory on the Cylinder Grating," Radiotekhnika i Electronika, Vol.21, no.3, pp.498-507 (1976) (in Russian).